MANAGEMENT SCIENCE
Vol. 56, No. 12, December 2010, pp. 2251–2264
ISSN 0025-1909 | EISSN 1526-5501 | 10 | 5612 | 2251

DOI 10.1287/mnsc.1100.1256

The Behavior of Risk and Market Prices of Risk Over the Nasdaq Bubble Period

Gurdip Bakshi
Smith School of Business, University of Maryland, College Park, Maryland 20742,
gbakshi@rhsmith.umd.edu

Liuren Wu
Zicklin School of Business, Baruch College, City University of New York, New York, New York 10010,
liuren.wu@baruch.cuny.edu

We exploit the information in the options market to study the variations of return risk and market prices of different sources of risk during the rise and fall of the Nasdaq market. We specify a model that accommodates fluctuations in both risk levels and market prices of different sources of risk, and we estimate the model using the time-series returns and option prices on the Nasdaq 100 tracking stock. Our analysis reveals three key variations during the period from March 1999 to March 2001. First, return volatility increased together with the rising Nasdaq index level, even though the two tend to move in opposite directions. Second, although the market price of diffusion return risk averages around 1.82 over the whole sample, the estimates reached negative territory at the end of 1999. The estimates reverted back to highly positive values after the collapse of the Nasdaq market. Third, the market price of jump risk increased with the rising Nasdaq valuation, and this increase in market price coincided with an increased imbalance in open interest between put and call options.

Key words: Nasdaq; risks; market prices of risk; diffusion risk; jump risk; open interest; options
History: Received January 17, 2009; accepted August 10, 2010, by Wei Xiong, finance.

1. Introduction

The Nasdaq market endured an unusual transformation at the turn of the 21st century. During the one-year period from March 1999 to March 2000, the Nasdaq 100 index, which constitutes the vast majority of the Nasdaq market capitalization, rose by 128%. Stock prices started to decline after that, and by March 2001 the level of the Nasdaq 100 index was about 30% of its peak value in 2000, a phenomenon labeled by many as the "Nasdaq bubble."

This paper provides a framework for analyzing the behavior of return risk and market prices of different sources of risk as revealed by option prices on the Nasdaq 100 tracking stock over the rise and fall of the Nasdaq.

In contrast to earlier bubbles, e.g., Dutch tulip mania and the South Sea bubble, the Nasdaq bubble segment incorporates a unique additional information source in the form of option quotes on the Nasdaq 100 tracking stock. Each day, option prices of different strikes and maturities provide us with a picture of the market's perception of the risk level and the conditional return distribution over different forward-looking horizons (Aït-Sahalia and Lo 1998, Birru and Figlewski 2009, Figlewski 2009). Thus, by analyzing the variations of the option prices and the underlying index, one can infer how the return risk and market prices of risk have varied during the bubble period.[1]

For this purpose, we specify a model that accommodates several distinct risk sources: (i) diffusion return risk, (ii) return volatility risk, (iii) upside jump risk, and (iv) downside jump risk. We assign a separate market price for each risk source, and we decompose the variations in the return risk premium into variations in the return risk level and in the market prices of different sources of risk. We also present an estimation procedure to extract the variations of return risk and market prices of risk from the option prices and the daily stock returns, while accounting for the correlation between option errors across option strikes and maturities.

Our model construction and estimation shows that return risk started to climb in late 1999 and spiked after the collapse of the Nasdaq. Return volatility calmed down during a short period in the middle of

[1] Ever since the classic works by Garber (1989) and Kindleberger (2000), bubbles and bursts have been a recurring theme of the financial market research. See, for instance, Abreu and Brunnermeier (2003), Battalio and Schultz (2006), Brunnermeier and Nagel (2004), Dhar and Goetzmann (2005), Griffin et al. (2004), Hong et al. (2006), Lakonishok et al. (2007), LeRoy (2004), Ofek and Richardson (2002, 2003), Pástor and Veronesi (2006), Schwert (2002), and Temin and Voth (2004).

2000 as the Nasdaq market experienced a short-lived recovery, but volatility rose again together with further deterioration in market capitalization.

Our estimation also identifies significant variations in the market prices of different sources of risk around the bubble period. The estimates for the market price for diffusion risk average around 1.82, close to common findings in the literature, but the estimates turned negative from September 21, 1999, to January 5, 2000, as the Nasdaq kept increasing. These negative estimates reflect a possible increase in the market's appetite for risk, and/or investors' subjective beliefs about future cash flows became much rosier than reality during this period.

We find that the market price of jump risk rose with the Nasdaq. The elevated market price of jump risk reflects put options becoming more expensive than call options during this period. This put–call price asymmetry is supported by a corresponding imbalance in the put–call open interest. On average, the open interest and trading volume are both higher for call options than for put options on the Nasdaq 100 tracking stock. However, the put open interest became much higher than the call open interest heading into the collapse of the Nasdaq.

Overall, our results show that the options market can provide an informative perspective about the development and analysis of financial bubbles and crises, and about how investors react to various sources of risk. Along the same lines, Birru and Figlewski (2009) provide insights on the most recent financial crisis of 2008 by analyzing the risk-neutral return densities implied by the S&P 500 index options.

The next section formalizes the model structure that decomposes the sources of return risk premium and characterizes the market prices of risk. Section 3 discusses the data, and §4 outlines the estimation procedure. Section 5 presents our estimation results on the behavior of the return risk and the market prices of risk, specific to the rise and the fall of the Nasdaq. Conclusions are offered in §6.

2. Risk Sources and Market Prices

We first decompose the index return into several risk sources and then assign a separate market price to each risk source. The decomposition of risk and market prices of risk, via a model, allows us to investigate whether risk levels and/or market prices of various sources of risk experienced systematic variations during the bubble period.

2.1. The Model Specification

Fix a filtered probability space $\{\Omega, \mathcal{F}, (\mathcal{F}_t)_{t\geq 0}, \mathbb{P}\}$, and let S_t be the level of the Nasdaq 100 tracking stock at time t. Assume that S_t is governed by the following stochastic differential equation:

$$\begin{aligned}\frac{dS_t}{S_{t-}} &= (\mathrm{rp}_t + (r_t - q_t))\,dt + \sqrt{V_t}\,dW_t \\ &\quad + \int_{\mathbb{R}^{0+}} (e^x - 1)(\mu_+[dx, dt] - V_t \pi_+[x]\,dx\,dt) \\ &\quad + \int_{\mathbb{R}^{0-}} (e^x - 1)(\mu_-[dx, dt] - V_t \pi_-[x]\,dx\,dt), \qquad (1)\end{aligned}$$

where S_{t-} denotes the time-t prejump level of the stock price. The instantaneous return dS_t/S_{t-} is decomposed into four components.

The first component includes the ex-dividend risk-free return $(r_t - q_t)$ and an instantaneous return risk premium rp_t. We allow the instantaneous interest rate r_t and the dividend yield q_t to evolve deterministically over time, and we derive the return risk premium based on our risk and market price specifications.

The second component captures the innovation of a continuous component, with dW_t denoting the change of a standard Brownian motion and V_t denoting its instantaneous variance rate, which varies stochastically according to the following stochastic differential equation:

$$dV_t = \kappa(\theta - V_t)\,dt + \omega\sqrt{V_t}\,dZ_t, \qquad (2)$$

where dZ_t denotes the change of another standard Brownian motion, correlated with the Brownian movement in the return by $\rho dt = \mathbb{E}^{\mathbb{P}}(dW_t dZ_t)$. Given this correlation, we can decompose the Brownian motion in the stock return into two components:

$$dW_t = \rho dZ_t + \sqrt{1-\rho^2}\,dB_t, \qquad (3)$$

where dB_t denotes the Brownian component in the stock return that is independent of the variance rate movement.

The third and fourth components in Equation (1) capture the contributions of upside and downside jumps, with $\mathbb{R}^{0+}$ and $\mathbb{R}^{0-}$ denoting the positive and negative halfs of the real line excluding zero, respectively. In particular, $\mu_+[dx, dt]$ and $\mu_-[dx, dt]$ count the number of upside and downside jumps of size x at time t, with $V_t\pi_+[x]dx\,dt$ and $V_t\pi_-[x]\,dx\,dt$ being the corresponding compensators for two types of jumps, respectively.

In the model, V_t governs not only the instantaneous variance rate of the Brownian movement, but also the arrival rate of upside and downside jumps. Furthermore, departing from Merton (1976), the model treats upside jumps and downside jumps separately, with $\pi_+[x]$ and $\pi_-[x]$ controlling the distribution of the upside and downside jumps, respectively.

We assume an exponential distribution for both types of jumps:

$$\pi_+[x] = \begin{cases} \lambda e^{-\beta_+ x} & x > 0, \\ 0 & x < 0; \end{cases}$$
$$\pi_-[x] = \begin{cases} 0 & x > 0, \\ \lambda e^{-\beta_- |x|} & x < 0, \end{cases} \tag{4}$$

where λ controls the mean arrival intensity, and β_+ and β_- control how fast the number of upside and downside jumps decrease with increasing jump sizes. The jump process has a stochastic arrival rate of $V_t\lambda(\beta_+^{-1}+\beta_-^{-1})$. Conditional on a jump occurring, the jump size x in log return has a double-exponential distribution as in Kou (2002).

Under our specification, the instantaneous stock return variance rate is $V_t(1+2\lambda(\beta_+^{-3}+\beta_-^{-3}))$, with the variance contribution from the diffusion component being V_t and the variance contribution from the jump component being $2V_t\lambda(\beta_+^{-3}+\beta_-^{-3})$.

To link the statistical dynamics to market prices of various sources of risk, we specify the dynamics of the state-price deflator $\mathcal{M}_t$ as

$$\begin{aligned}\frac{d\mathcal{M}_t}{\mathcal{M}_{t-}} &= -r_t dt - \gamma_B\sqrt{V_t}\,dB_t - \gamma_Z\sqrt{V_t}\,dZ_t \\ &\quad - \gamma_{J+}\int_{\mathbb{R}^{0+}}(e^x-1)(\mu_+[dx,dt]-V_t\pi_+[x]dx\,dt) \\ &\quad - \gamma_{J-}\int_{\mathbb{R}^{0-}}(e^x-1)(\mu_-[dx,dt]-V_t\pi_-[x]dx\,dt). \end{aligned}\tag{5}$$

The specification assigns a separate market price for each of the four sources of risk: the independent diffusive return risk (γ_B), the diffusion variance risk (γ_Z), the upside jump risk (γ_{J+}), and the downside jump risk (γ_{J-}).

The market prices of different sources of risk capture the differences between the risk-neutral dynamics $\mathbb{Q}$ and the statistical dynamics $\mathbb{P}$ as a result of (i) investors' risk aversions to different sources of risk and/or (ii) deviations of investors' subjective beliefs from statistical realities. We identify these market prices without making a distinction between the two explanations.

Our model is in line with extant literature and is designed to address the question of how the market prices of different risk sources changed during the Nasdaq bubble period. Earlier works, e.g., Bakshi et al. (1997) and Huang and Wu (2004), often combine Heston's (1993) stochastic volatility specification with Merton's (1976) jump diffusion. The double-exponential specification of Kou (2002) in Equation (4) provides an attractive alternative to the Merton (1976) model, while allowing us to consider the distinct pricing of downside and upside jumps.

2.2. The Return Risk Premium Decomposition

Under our specification of risk dynamics and market prices of different sources of risk, we can decompose the return risk premium into two components: the return risk level as captured by the variance rate V_t and the risk premium per unit risk. We can further attribute the risk premium per unit risk to contributions from diffusion risks and contributions from jump risks.

Theorem 1. *Under the price dynamics in* (1)–(3) *and the state-price deflator dynamics in* (5), *the instantaneous return risk premium is* $\mathrm{rp}_t = \eta V_t$, *where* V_t *measures the time-t return risk level, and* η *measures the risk premium per unit risk. The per-unit risk premium* η *can be decomposed further into contributions from diffusion risks* (η_d) *and jump risks* (η_J):

$$\eta = \eta_d + \eta_J, \tag{6}$$

with

$$\eta_d = \gamma_B\sqrt{1-\rho^2} + \gamma_Z\rho, \tag{7}$$

$$\begin{aligned}\eta_J &= \lambda(((\beta_+-1)^{-1}-\beta_+^{-1})+((\beta_-+1)^{-1}-\beta_-^{-1})) \\ &\quad - \lambda(((\beta_+ + \gamma_{J+}-1)^{-1}-(\beta_+ + \gamma_{J+})^{-1}) \\ &\quad + ((\beta_- - \gamma_{J-}+1)^{-1}-(\beta_- - \gamma_{J-})^{-1})). \end{aligned}\tag{8}$$

Conditional on a fixed return risk level, the diffusion risk premium is given by the negative of the covariance between the diffusion innovations in the return and the state-price deflator,

$$\begin{aligned}\eta_d &\equiv \frac{1}{V_t\,dt}\mathbb{E}^{\mathbb{P}}(\sqrt{V_t}dW_t(\gamma_B\sqrt{V_t}\,dB_t + \gamma_Z\sqrt{V_t}dZ_t)) \\ &= \gamma_B\sqrt{1-\rho^2} + \gamma_Z\rho, \end{aligned}\tag{9}$$

which captures the contribution from both the return risk B_t and the variance risk Z_t. The jump risk premium is obtained by performing the integration (e.g., Küchler and Sørensen 1997)

$$\begin{aligned}\eta_J &= \int_{\mathbb{R}^{0+}}(e^x-1)(1-e^{-\gamma_{J+}x})\pi_+[x]\,dx \\ &\quad + \int_{\mathbb{R}^{0-}}(e^x-1)(1-e^{-\gamma_{J-}x})\pi_-[x]\,dx, \end{aligned}\tag{10}$$

the magnitude of which is determined by the market prices of upside and downside jumps γ_{J+} and γ_{J-}, respectively.

The market price of the diffusion return risk, γ_B, generates a return risk premium as in Merton (1976). In addition, the market price of diffusion variance risk γ_Z also contributes to the diffusion return risk premium η_d through its correlation with the return innovation. Furthermore, the market prices of upside and downside jump risks (γ_{J+} and γ_{J-}) induce additional risk premiums in the form of η_J in (8). Finally, stochastic volatility renders the risk premium stochastic as the risk premium is proportional to the variance rate V_t.

Equation (7) suggests that a positive market price of return risk (γ_B) generates a positive return risk premium. Furthermore, when the return and the variance rate has a negative correlation ($\rho < 0$), a positive return risk premium can also result from a negative market price of variance risk ($\gamma_Z < 0$). Positive market prices for jump risks generate a positive return risk premium, as reflected in Equation (8).

Unlike the traditional focus on the behavior of total return risk premium in some early studies of bubbles and bursts, the risk premium decomposition in Theorem 1 is imperative to our analysis. The first question to ask is whether a risk premium change is due to a change in return risk level (V_t) or a change in its market price (the risk premium per unit return risk, η). Our explicit distinction and separate estimation of the two components are important for understanding how the return risk level and the market price per unit risk had varied separately during the bubble period.

Second, by classifying the different risk sources and assigning a different market price to each risk source, we can go one step further in documenting the different variations of the market prices on different risk sources over the Nasdaq bubble period. In this sense, our goals are aligned with those of Bollerslev and Todorov (2009) and Santa-Clara and Yan (2010), who study the time variation in risk premiums, and with those of Figlewski (2009), who analyzes the variation of the risk-neutral density of the S&P 500 index return over the 2008 crisis period.[2]

2.3. The Information Content in Option Prices

Given the state-price deflator specification in (5), the price dynamics under the risk-neutral measure $\mathbb{Q}$ can be written as (Küchler and Sørensen 1997)

$$\begin{aligned} dS_t/S_{t-} &= (r_t - q_t)\,dt + \sqrt{V_t}\,dW_t^{\mathbb{Q}} \\ &\quad + \int_{\mathbb{R}^{0+}} (e^x - 1)(\mu_+[dx, dt] - V_t \pi_+^{\mathbb{Q}}[x]\,dx\,dt) \\ &\quad + \int_{\mathbb{R}^{0-}} (e^x - 1)(\mu_-[dx, dt] - V_t \pi_-^{\mathbb{Q}}[x]\,dx\,dt), \end{aligned} \tag{11}$$

where $\pi_+^{\mathbb{Q}}[x]$ and $\pi_-^{\mathbb{Q}}[x]$ are exponential tilted versions of their statistical counterparts,

$$\pi_+^{\mathbb{Q}}[x] = \begin{cases} \lambda e^{-(\beta_+ + \gamma_{J+})x} & x > 0, \\ 0 & x < 0; \end{cases}$$
$$\pi_-^{\mathbb{Q}}[x] = \begin{cases} 0 & x > 0, \\ \lambda e^{-(\beta_- - \gamma_{J-})|x|} & x < 0, \end{cases} \tag{12}$$

[2] See also, among others, Bliss and Panigirtzoglou (2004), Bollen and Whaley (2004), Huang and Wu (2004), Jones (2006), Bakshi et al. (2008), Li et al. (2008), and Christoffersen et al. (2008).

from which we can define the risk-neutral dampening coefficients as

$$\beta_+^{\mathbb{Q}} \equiv \beta_+ + \gamma_{J+} \quad \text{and} \quad \beta_-^{\mathbb{Q}} \equiv \beta_- - \gamma_{J-}. \tag{13}$$

Positive market prices on the two jump risks increase the dampening on upside jumps but reduce the dampening on downside jumps. As a result, the return innovation distribution becomes more negatively skewed under the risk-neutral measure $\mathbb{Q}$.

The risk-neutral dynamics of the instantaneous variance rate in our setting become

$$dV_t = \kappa^{\mathbb{Q}}(\theta^{\mathbb{Q}} - V_t)\,dt + \omega\sqrt{V_t}\,dZ_t^{\mathbb{Q}}, \tag{14}$$

with $\kappa^{\mathbb{Q}} \equiv \kappa + \gamma_Z\omega$ and $\theta^{\mathbb{Q}} \equiv \kappa\theta/\kappa^{\mathbb{Q}}$. A negative market price of variance risk reduces the risk-neutral mean-reversion speed and increases the risk-neutral mean of the variance rate.

The Fourier transform of the log return under the risk-neutral measure $\mathbb{Q}$ is exponential affine in the variance rate V_t,

$$\begin{aligned} &\phi^{\mathbb{Q}}[u; V_t, \Theta] \\ &\quad \equiv \mathbb{E}_t^{\mathbb{Q}}(e^{iu(\ln S_{t+\tau}/S_t)}) \\ &\quad = \exp\left(iu\int_t^{t+\tau}(r_s - q_s)ds - a^{\mathbb{Q}}[\tau] - b^{\mathbb{Q}}[\tau]V_t\right), \\ &\qquad\qquad u \in \mathbb{D} \in \mathbb{C}, \end{aligned} \tag{15}$$

where Θ denotes the parameter set, and the coefficients $a^{\mathbb{Q}}[\tau]$ and $b^{\mathbb{Q}}[\tau]$ are functions of the parameters that govern the return risk dynamics and market prices of risk,

$$\begin{aligned} a^{\mathbb{Q}}[\tau] &= \frac{2\kappa\theta}{\omega^2}\ln\left(1 - \frac{\vartheta^{\mathbb{Q}} - \kappa^{\mathbb{M}}}{2\vartheta^{\mathbb{Q}}}(1 - e^{-\vartheta^{\mathbb{Q}}\tau})\right) \\ &\quad - \frac{\kappa\theta}{\omega^2}(\vartheta^{\mathbb{Q}} - \kappa^{\mathbb{M}})\tau, \\ b^{\mathbb{Q}}[\tau] &= \frac{2\psi^{\mathbb{Q}}(1 - e^{-\vartheta^{\mathbb{Q}}\tau})}{2\vartheta^{\mathbb{Q}} - (\vartheta^{\mathbb{Q}} - \kappa^{\mathbb{M}})(1 - e^{-\vartheta^{\mathbb{Q}}\tau})}, \end{aligned} \tag{16}$$

with $\kappa^{\mathbb{M}} \equiv \kappa + \gamma_Z\omega - iu\omega\rho$, $\vartheta^{\mathbb{Q}} \equiv \sqrt{(\kappa^{\mathbb{M}})^2 + 2\omega^2\psi^{\mathbb{Q}}}$, and $\psi^{\mathbb{Q}}$ the risk-neutral characteristic exponent of the standardized log return innovation with V_t fixed at unity:

$$\begin{aligned} \psi^{\mathbb{Q}} &= \tfrac{1}{2}(iu + u^2) \\ &\quad - \lambda\big(((\beta_+ + \gamma_{J+} - iu)^{-1} - (\beta_+ + \gamma_{J+})^{-1}) \\ &\qquad + iu((\beta_+ + \gamma_{J+} - 1)^{-1} - (\beta_+ + \gamma_{J+})^{-1})\big) \\ &\quad - \lambda\big(((\beta_- - \gamma_{J-} + iu)^{-1} - (\beta_- - \gamma_{J-})^{-1}) \\ &\qquad + iu((\beta_- - \gamma_{J-} + 1)^{-1} - (\beta_- - \gamma_{J-})^{-1})\big). \end{aligned} \tag{17}$$

Given the Fourier transform in (15), we can numerically compute the time-t values of options with time to maturity τ via fast Fourier inversion, as proposed in Carr and Madan (1999) and Carr and Wu (2004).

Equations (15)–(17) show that the option value depends on the return risk level V_t as well as the parameters that govern the price and variance rate dynamics and the market prices of risk. We can use the observed option prices across different strikes and maturities each day to infer the return risk level and the market prices on that date.

2.4. The Information Content in Stock Returns

Time-series observations of returns provide additional information on the price dynamics, as revealed through the likelihood or, equivalently, the conditional probability density of the returns.

To incorporate this information in our estimation, let $\ln S_{t+h}/S_t$ denote the time-t log return over a sampling frequency of h. Analogous to (15), the return characteristic function under measure $\mathbb{P}$ is

$$\begin{aligned}\phi^{\mathbb{P}}[u; V_t, \Theta] &\equiv \mathbb{E}_t^{\mathbb{P}}(e^{iu(\ln S_{t+h}/S_t)}) \\ &= \exp(iurh - a^{\mathbb{P}}[h] - b^{\mathbb{P}}[h]V_t), \quad u \in \mathbb{R}, \end{aligned} \tag{18}$$

where

$$\begin{aligned} a^{\mathbb{P}}[h] &= \frac{2\kappa\theta}{\omega^2}\ln\left(1 - \frac{\vartheta^{\mathbb{P}} - \kappa^{\mathbb{N}}}{2\vartheta^{\mathbb{P}}}(1 - e^{-\vartheta^{\mathbb{P}}h})\right) \\ &\quad - \frac{\kappa\theta}{\omega^2}(\vartheta^{\mathbb{P}} - \kappa^{\mathbb{M}})h, \\ b^{\mathbb{P}}[h] &= \frac{2\psi^{\mathbb{P}}(1 - e^{-\vartheta^{\mathbb{P}}h})}{2\vartheta^{\mathbb{P}} - (\vartheta^{\mathbb{P}} - \kappa^{\mathbb{N}})(1 - e^{-\vartheta^{\mathbb{P}}h})}, \end{aligned} \tag{19}$$

with $\kappa^{\mathbb{N}} \equiv \kappa - iu\omega\rho$, $\vartheta^{\mathbb{P}} \equiv \sqrt{(\kappa^{\mathbb{N}})^2 + 2\omega^2\psi^{\mathbb{P}}}$, and

$$\begin{aligned} \psi^{\mathbb{P}} &= iu\eta + \tfrac{1}{2}(iu + u^2) \\ &\quad - \lambda\big(((\beta_+ - iu)^{-1} - (\beta_+)^{-1}) \\ &\qquad + iu((\beta_+ - 1)^{-1} - (\beta_+)^{-1})\big) \\ &\quad - \lambda\big(((\beta_- + iu)^{-1} - (\beta_-)^{-1}) \\ &\qquad + iu((\beta_- + 1)^{-1} - (\beta_-)^{-1})\big). \end{aligned} \tag{20}$$

Conditional on the variance rate level V_t, we can apply fast Fourier transform to the return characteristic function in Equation (18) to obtain the corresponding conditional probability density.

3. Data on the Nasdaq Tracking Stock and Options

We estimate the risk dynamics and market prices of risk using both the time-series returns and option prices on the Nasdaq 100 tracking stock. The Nasdaq 100 index captures the vast majority of the Nasdaq market capitalization and strongly comoves with the Nasdaq composite index. For estimation, we sample the data daily from March 17, 1999, to February 19, 2003.

Daily log returns on the index tracking stock are computed based on daily closing dividend-adjusted prices. The time series of excess log returns is obtained by subtracting the overnight London Interbank Offered Rate (LIBOR) from the daily returns.

Options on the Nasdaq 100 tracking stock are actively traded. We obtain the options data from the "Ivy DB" data set sold by OptionMetrics. Because these options are American style, OptionMetrics employs a binomial tree approach to adjust for the early exercise feature in calculating the implied volatility from the daily closing midquote of the option.

Put–call parity dictates that the put and the call options at the same strike and maturity should generate the same implied volatility. At times, OptionMetrics generates two different implied volatilities when its assumptions on the interest rate curve, the dividend schedule, and the borrow cost differ from the market (see also Lamont and Thaler 2003). To rectify this aberration, we choose, at each maturity, the strike closest to the spot price and measure the difference between the OptionMetrics implied volatility estimates for the call and the put options. Then, we add half of the difference to call implied volatility estimates and deduct half of the difference to put implied volatility estimates. Through this adjustment, the implied volatilities corresponding to the put and the call at the strike closest to the spot price become identical to each other. At other strikes, we take the adjusted implied volatility of the out-of-the-money (OTM) options, i.e., the call option when the strike is above the spot, and the put option when the strike is below the strike.

We convert the implied volatility at each strike and maturity into the corresponding OTM European option value according to the Black and Scholes (1973) pricing formula. The forward price is computed based on the interest rate curve and the dividend projection provided by OptionMetrics.

Similar to extant practices (e.g., see the details in Figlewski 2009), we apply three additional filters to the data in constructing the daily options sample. First, the bid price is greater than zero. Second, the option maturity is no less than ten days and no more than one year. Third, the strikes of the options are confined to two standard deviations of the forward. The procedure generates 159,218 option prices over 987 business days.

Table 1 displays summary information on the time series of the Nasdaq 100 tracking stock and its daily returns in panel A, and on the options sample in panel B. Panel A shows that the average price of the Nasdaq 100 tracking stock is \$53.32 over our sample period from March 17, 1999, to February 19, 2003. The lowest level is \$19.55, and the highest level is \$114.74. The daily return has a standard deviation of 3.01% per day, with the largest single day percentage

Table 1 Descriptive Statistics on Nasdaq 100 Tracking Stock and Its Options

	Average	SD	Min	Max
A. Nasdaq 100 tracking stock				
Index level ($)	53.32	24.71	19.55	114.74
Daily return (%)	−0.07	3.01	−9.06	15.57
B. Options on the Nasdaq 100 tracking stock				
Number of calls per day	71	38	0	176
Number of puts per day	90	48	20	235
Days to expiration	129	85	10	365
Call implied volatility (%)	43.43	8.26	24.82	95.52
Put implied volatility (%)	50.56	9.54	27.67	108.36

Notes. Entries report summary statistics on the Nasdaq 100 tracking stock and its daily returns in panel A and the options sample in panel B over the period from March 17, 1999, to February 19, 2003 (987 business days). Daily log stock returns on the Nasdaq 100 index are computed based on daily closing dividend-adjusted prices. Options data are from OptionMetrics, which computes the options implied volatilities based on a binomial tree. The options sample is selected according to the following criteria: (i) the bid price is greater than zero, (ii) the option maturity is between 10 days and one year, (iii) the strikes of the options are confined to two standard deviations of the forward, and (iv) the out-of-the-money option is chosen at each strike and maturity. The selection criteria yield a total of 159,218 observations, among which 70,185 are calls and 89,033 are puts.

return drop at −9.06% and the largest single day spike at 15.57%.

Panel B shows that, on average, 71 call options and 90 put options are used per day for the estimation. Over time, the number of calls per day varies from zero to 176, and the number of puts per day varies from 20 to 235. We filter the options to have maturities of no less than 10 days and no more than 365 days, with an average maturity of 129 days. The Black and Scholes (1973) implied volatilities for calls average at 43.43% and vary from 24.82% to 95.52%. The put implied volatilities are higher, with an average of 50.56%, a minimum of 27.67%, and a maximum of 108.36%.

In Table 2 we divide the options sample into six moneyness and four maturity regions, and report the average statistics in each of the 24 moneyness/maturity regions. Maturity is measured in number of actual days, and moneyness is in absolute percentage log strike deviation from forward, $|\ln(K/F)|$, where K is the strike price, and F is the forward. Panel A reports the average daily open interest in each region, and panel B reports the average daily trading volume. Over our sample period, the average open interest and trading volume on OTM calls are higher than their put counterparts. Furthermore, trading volume and open interest are concentrated in options with maturities within six months, with trading activities waning thereafter.

Panel C of Table 2 reports the average implied volatility across different moneyness and maturity regions. At short maturities (10–90 days), the average implied volatility is U-shaped in moneyness. At longer maturities, the moneyness relation becomes downward sloping, with the average implied volatilities at low strikes higher than the average implied volatilities at high strikes.

4. The Maximum Likelihood Estimation

Our model features stochastic volatility, a separation of up and down jumps, and stochastically varying risk

Table 2 Options Open Interest, Volume, and Implied Volatility by Maturity and Moneyness

	Nasdaq 100 puts (%)			Nasdaq 100 calls (%)		
$\lvert\ln(K/F)\rvert$, % Days to expiration:	>10	5–10	0–5	0–5	5–10	> 10
A. Average daily open interest (number of contracts)						
10–45	84,667	50,663	58,903	61,201	64,002	112,588
45–90	61,657	20,907	22,273	22,303	24,112	94,952
90–180	63,624	17,021	18,098	18,817	20,785	113,961
180–365	39,309	9,094	8,505	9,000	9,076	85,631
B. Average daily volume (number of contracts)						
10–45	6,948	8,849	14,700	17,679	10,802	8,663
45–90	3,761	2,039	2,838	3,228	2,442	5,035
90–180	2,339	1,056	1,202	1,255	1,220	3,143
180–365	1,385	366	588	465	411	1,801
C. Average implied volatility (%)						
10–45	58.70	49.34	46.67	45.10	45.50	50.78
45–90	55.80	46.65	45.08	44.21	44.68	46.37
90–180	51.09	44.20	43.21	42.56	42.84	42.30
180–365	48.87	43.48	42.43	41.84	41.87	39.28

Notes. Entries report summary statistics on the Nasdaq 100 options by maturity and moneyness over the daily sample period from March 17, 1999, to February 19, 2003 (987 business days). The data are from OptionMetrics. Maturity is in number of actual days, and moneyness is defined as $|\ln(K/F_{t,T})|$, where $F_{t,T}$ is the forward price and K is the strike.

premia on each type of risk. The aim of this section is to present a procedure to estimate the risk dynamics V_t jointly with the market prices of risk, based on the daily time series of returns and option prices on the Nasdaq 100 tracking stock.

We estimate the model parameters by maximizing the joint likelihood of the option prices and daily returns. To construct the likelihood function, we cast the model into a state-space form and extract the distributions of the states at each date using a filtering technique.

4.1. The Propagation Equations

Our base model assumes that all the market prices of risk coefficients $(\gamma_Z, \gamma_B, \gamma_{J+}, \gamma_{J-})$ are constant. In this case, we regard the instantaneous variance rate as the state $X_t = V_t$. The state propagation equation is determined by the statistical dynamics of the variance rate in Equation (2).

To analyze the return risk and risk premium variation around the rise and fall of the Nasdaq, we extend the base model to accommodate time-varying market prices for different sources of risk. In this extension, we use $z_t \equiv (\gamma_Z, \ln\beta_+^{\mathbb{Q}}, \ln\beta_-^{\mathbb{Q}})$ to denote the additional state variables that we allow to vary over time, and we use $X_t = (V_t, z_t)$ as the expanded state vector. We retain the assumption of a constant market price of return risk γ_B, because its identification comes mainly from the daily returns, and options provide little information on inferring this coefficient. Furthermore, with (β_+, β_-) fixed, we use the variation of $(\beta_+^{\mathbb{Q}}, \beta_-^{\mathbb{Q}})$ to reflect the variation in the market prices of upside and downside jumps $(\gamma_{J+}, \gamma_{J-})$, with $\gamma_{J+} = \beta_+^{\mathbb{Q}} - \beta_+$ and $\gamma_{J-} = \beta_- - \beta_-^{\mathbb{Q}}$. The log transformation of $\beta_+^{\mathbb{Q}}$ and $\beta_-^{\mathbb{Q}}$ expands the domain of the two coefficients to the whole real line.

We specify the following auxiliary dynamics for $z_t = (\gamma_Z, \ln\beta_+^{\mathbb{Q}}, \ln\beta_-^{\mathbb{Q}})^\top$:

$$z_t = (1-\varphi_z)\theta_z + \varphi_z z_{t-1} + \sigma_z \zeta_t, \tag{21}$$

where $\theta_z = (\overline{\gamma_Z}, \overline{\ln\beta_+^{\mathbb{Q}}}, \overline{\ln\beta_-^{\mathbb{Q}}})^\top$ denotes the long-run mean vector. We also use two auxiliary coefficients, φ_z and σ_z, to capture the mean reversion speed and variance of z_t, respectively, with ζ_t denoting a standardized normal vector.

To avoid the complication of convexity terms for option pricing, we take the market prices as deterministically time varying and treat Equation (21) as a conditional forecasting equation analogous to the generalized autoregressive conditional heteroskedasticity (GARCH) specification for volatilities (Engle 1982, Bollerslev 1986). Hence, the filtered updates on z_t can be regarded as time-t forecasts of future market prices of risk.

For both constant and time-varying market prices of risk specifications, we can write the state propagation equation generically as

$$X_t = A + \Phi X_{t-1} + \sqrt{\mathbb{Q}_{t-1}}\,\xi_t, \tag{22}$$

where ξ_t is an independent and identically distributed (i.i.d.) standard normal innovation vector, and $\mathbb{Q}_{t-1}$ denotes the conditional covariance matrix of the innovation.

When $X_t = V_t$, Equation (22) represents a discretized version of the continuous-time dynamics of V_t in (2), with $A = (1-e^{-\kappa h})\theta$, $\Phi = e^{-\kappa h}$, $\mathbb{Q}_{t-1} = \omega^2 V_{t-1} h$, and $h = 1/252$ denoting the daily time interval used in our estimation. When $X_t = (V_t, z_t)$, the state propagation equation is expanded accordingly, with $A = [(1-e^{-\kappa h})\theta, (1-\varphi_z)\theta_z]$, Φ indicating a diagonal matrix with the diagonal elements given by $(e^{-\kappa h}, \varphi_z \mathbf{e}_3)$, $\mathbf{e}_3$ denoting a three-dimensional vector of ones, and $\mathcal{G}_{t-1}$ also indicating a diagonal matrix with the diagonal elements given by $(\omega^2 V_{t-1} h, \sigma_z^2 \mathbf{e}_3)$.

4.2. The Measurement Equations

The measurement equations are constructed based on the observed OTM option prices, assuming additive, normally distributed measurement errors. Let y_t denote these observed option prices at time t, and let $\mathcal{O}[X_t; \Theta]$ denote their corresponding model values as a function of the state level X_t and the model parameters Θ. We can write the measurement equation as

$$y_t = \mathcal{O}[X_t; \Theta] + e_t, \tag{23}$$

with e_t denoting the measurement error.

Because the exchange-listed option contracts have fixed strikes and fixed expirations, the moneyness and time to maturity of each contract varies daily as time passes by and as the spot level changes. Furthermore, with old contracts expiring and new contracts being issued, the number of option contracts, and hence the dimension of the measurement equation, varies over time. These variations make it difficult to estimate a generic covariance matrix for the measurement errors e_t in Equation (23).

To make the estimation steps tractable in our context, we first represent each OTM option price as a percentage of the underlying spot level, and then scale this value by the vega of the option as in Bakshi et al. (2008). With this scaling, we assume that the scaled measurement errors on all option contracts have the same error variance. As option values vary with moneyness and maturity, so do the measurement errors. The rationale for vega scaling is to make option values more comparable across moneyness and maturity, thereby facilitating the simplifying assumption of identical error variance.

4.3. Adjusting for Cross-Dependence and Serial Dependence in Measurement Errors

Measurement errors on different option contracts are likely to be correlated. We capture this correlation

of the measurement errors between contracts i and j through the following functional form:

$$\rho_{ij} = \max\left(0, 1 - \frac{|D_i - D_j|}{g_d}\right) \cdot \max\left(0, 1 - \frac{|\tau_i - \tau_j|}{g_m}\right), \quad (24)$$

where D denotes the Black and Scholes (1973) delta of the option, and τ denotes the option maturity in years. Intuitively, as the distance between the two contracts in terms of moneyness and maturity increases, the correlation declines. The two positive scaling parameters g_d and g_m control the speed of decline along the two dimensions, respectively. We treat the two scaling coefficients as free parameters and determine their value through the maximum likelihood estimation.

Furthermore, a positive measurement error today is likely to be followed by a positive measurement error tomorrow on the same contract. To rectify the impact of serial dependence on our estimation, we assume the following error structure for each contract i:

$$e_t^i = \rho_e e_{t-1}^i + \sigma_e \varepsilon_t^i, \quad (25)$$

where we posit the same serial correlation ρ_e and error variance σ_e^2 on all option contracts, with ε_t^i denoting an i.i.d standard normal variable. The two coefficients ρ_e and σ_e are estimated within our maximum likelihood procedure.

With these assumptions, we can build the covariance matrix of the measurement errors $\mathcal{R}_{t-1}$ at each date t.

4.4. The Filtering Procedure

Let $\overline{X}_t$, $\bar{\Sigma}_{X,t}$, $\bar{y}_t$, $\bar{\Sigma}_{y,t}$ denote the time-$(t-1)$ forecasts of time-t values of the state, the covariance matrix of the state, the measurement series, and the covariance matrix of the measurement series, respectively, and let $\widehat{X}_t$ and $\hat{\Sigma}_{X,t}$ denote the ex post updates on the state vector and the state covariance based on observations y_t at time t.

Given the Gaussian linear structure of the state-propagation equation in (22), we generate the state predictions analytically as

$$\overline{X}_t = A + \Phi \widehat{X}_{t-1}, \qquad \bar{\Sigma}_{X,t} = \Phi \hat{\Sigma}_{X,t-1} \Phi^\top + \mathcal{Q}_{t-1}. \quad (26)$$

In the case of linear measurement equations of the form $y_t = HX_t + e_t$, the predicted values of the measurements and their covariances can also be computed analytically:

$$\bar{y}_t = H\overline{X}_t, \quad \bar{\Sigma}_{y,t} = H\bar{\Sigma}_{X,t}H^\top + \mathcal{R}_{t-1}, \quad \bar{\Sigma}_{Xy,t} = \bar{\Sigma}_{X,t}H^\top. \quad (27)$$

The filtering of the states can be performed according to the classic Kalman (1960) filter,

$$\widehat{X}_t = \overline{X}_t + K_t(y_t - \bar{y}_t), \quad \hat{\Sigma}_{X,t} = \bar{\Sigma}_{X,t} - K_t \bar{\Sigma}_{y,t} K_t^\top, \quad (28)$$

where K_t is the Kalman gain, given by $K_t = \bar{\Sigma}_{Xy,t}(\bar{\Sigma}_{y,t})^{-1}$.

In our application, the measurement equation in (23) is nonlinear. We use the unscented Kalman filter (Wan and van der Merwe 2001) to handle this nonlinearity. Under this approach, we first approximate the distribution of the state vector using a set of deterministically chosen sigma points and then propagate these sigma points through the nonlinear measurement equation.

Specifically, let p be the number of states, $\delta > 0$ be a control parameter, and Σ_i be the ith column of a matrix Σ. A set of $2p+1$ sigma vectors χ_i are generated based on the conditional mean and covariance forecasts on the state vector according to the equations

$$\chi_{t,0} = \overline{X}_t, \quad \chi_{t,i} = \overline{X}_t \pm \sqrt{(p+\delta)(\bar{\Sigma}_{X,t})_j}, \quad j = 1, \ldots, p;\ i = 1, \ldots, 2p, \quad (29)$$

with corresponding weights w_i given by

$$w_0 = \delta/(p+\delta), \quad w_i = 1/[2(p+\delta)], \quad j = 1, \ldots, 2p. \quad (30)$$

We can regard these sigma vectors as forming a discrete distribution, taking w_i the corresponding probabilities. Given the sigma points, we can compute the predicted values of the measurements and their covariances as

$$\bar{y}_t = \sum_{i=0}^{2p} w_i \mathcal{O}[\bar{\chi}_{t,i}; \Theta],$$

$$\bar{\Sigma}_{y,t} = \sum_{i=0}^{2p} w_i [\mathcal{O}[\bar{\chi}_{t,i}; \Theta] - \bar{y}_t][\mathcal{O}[\bar{\chi}_{t,i}; \Theta] - \bar{y}_t]^\top + \mathcal{R}_{t-1}, \quad (31)$$

$$\bar{\Sigma}_{Xy,t} = \sum_{i=0}^{2p} w_i (\bar{\chi}_{t,i} - \overline{X}_t)(\mathcal{O}[\bar{\chi}_{t,i}; \Theta] - \bar{y}_t)^\top.$$

With the conditional mean and covariance computed from the sigma points, we can apply the Kalman (1960) filter in Equation (28) to update the states and their covariances.

4.5. The Joint Log-Likelihood from Options and Index Returns

The unscented Kalman filter is applied to the options data sequentially from the first day to the last day of the observation. With the filtering results, we construct the log-likelihood for each day's option observations by assuming that the forecasting errors are normally distributed:

$$l_t^O[\Theta] = -\tfrac{1}{2}\log|\bar{\Sigma}_{y,t}| - \tfrac{1}{2}((y_t - \bar{y}_t)^\top (\bar{\Sigma}_{y,t})^{-1}(y_t - \bar{y}_t)). \quad (32)$$

Furthermore, conditional on the state vector filtered from the options, we compute the conditional probability density of the log return, $f[x; V_t, \Theta] = \frac{1}{\pi}\int_0^\infty e^{-iux}\phi_t^{\mathbb{P}}[u; V_t, \Theta]\,du$, through the fast Fourier inversion of the characteristic function ($\phi_t^{\mathbb{P}}[u; V_t, \Theta]$) in Equation (18). We first compute the probability density numerically on a fine grid of return values x, and then map the grid to the realized return on that day, $\ln S_{t+1}/S_t$, to obtain the conditional probability density of the realized return, $f[\ln S_{t+1}/S_t; V_t, \Theta]$. Then, we compute the conditional log-likelihood of the daily return as

$$l_t^s[\Theta] = \ln f[\ln S_{t+1}/S_t; V_t, \Theta]. \tag{33}$$

Finally, assuming conditional independence between the options forecasting errors and the daily returns, we construct the joint daily log-likelihood as the sum of the log-likelihoods from the two data sources in (32) and (33), respectively. We choose model parameters to maximize the joint log-likelihoods from both options and daily returns,

$$\max_{\Theta}\sum_{t=1}^{T}(l_t^O[\Theta] + l_t^s[\Theta]), \tag{34}$$

where $T = 987$ denotes the number of days in our sample.

5. Risk and Market Price Variations During the Bubble Period

Through model estimation, we extract the variation of the return variance rate (V_t), as a measure of the return risk level, and the market prices of different sources of risk on the Nasdaq 100 tracking stock. We document how they vary during the rise and fall of the Nasdaq market.

We have estimated models with both constant and time-varying market prices of risk. The two models generate similar parameter estimates and return variances, confirming the robustness of our specifications and estimation methodology. For ease of exposition, we focus on the model with time-varying market prices of risk, with parameter estimates reported in Table 3. We also provide the parameter estimates under constant market prices in the appendix. The parameter estimates in panel D in both tables show the relevance of accounting for cross-correlations and serial correlations among the measurement errors on the options.

5.1. Return Volatility Increased with Nasdaq 100 Valuation

Panel A of Table 3 presents the estimates of parameters governing the variance rate dynamics in (2), with the corresponding t-statistics in parenthesis. The

Table 3 Model Parameter Estimates Under Time-Varying Market Prices of Risk

A. Variance risk dynamics				
	κ	θ	ω	ρ
Coef.	9.2169	0.1179	0.7927	−0.8389
t-statistic	(12.88)	(13.18)	(75.49)	(−72.66)

B. Jump risk dynamics			
	λ	β_+	β_-
Coef.	26.0210	19.2990	15.6960
t-statistic	(48.44)	(0.80)	(0.59)

C. Market prices of diffusion and jump risks						
	$\overline{\gamma_Z}$	$\overline{\ln\beta_+^{\mathbb{Q}}}$	$\overline{\ln\beta_-^{\mathbb{Q}}}$	γ_B	φ_z	σ_z^2
Coef.	−1.4325	10.330	7.5920	1.1209	0.9909	0.0094
t-statistic	(−1.69)	(5.70)	(3.26)	(0.67)	(1,030.16)	(23.01)

D. Cross-sectional and serial dependence in measurement errors				
	g_d	g_m	ρ_e	σ_e^2
Coef.	1.1321	0.0731	0.4049	0.0408
t-statistic	(704.70)	(0.00)	(130.12)	(245.89)

Notes. Entries report the maximum likelihood estimates of the model parameters with time-varying market prices of risk. The t-statistics are shown in parentheses. The estimation is based on daily time-series returns and option prices on Nasdaq 100 tracking stock over the sample period from March 17, 1999, to February 19, 2003. Likelihoods on options are constructed by assuming normally distributed options forecasting errors, with the mean and covariance of the forecasts obtained from the unscented Kalman filter. Likelihoods on daily returns are computed by inverting the characteristic function of the daily return, conditional on the variance rate extracted from the options. The joint likelihood is obtained by assuming independence between options forecasting errors and daily stock returns.

parameters of the variance dynamics are estimated with a high degree of statistical significance, suggesting that the estimation procedure is successful in identifying the evolution of return volatility.

The estimate for the variance of variance coefficient ω is large at 0.7927, suggesting that the return variance itself is highly volatile. The estimate for the speed of mean-reversion coefficient κ is also large at 9.2169, implying quick mean reversion in the Nasdaq volatility variation. The long-run mean (θ) estimate of 0.1179 represents an average volatility level of 34.68%, computed as $\sqrt{\theta(1+2\lambda(\beta_+^{-3}+\beta_-^{-3})}$. Last, the diffusion component of the return innovation and the variance innovation have a strongly negative correlation at $\rho=-0.8389$, which contributes to the implied volatility skew observed at moderate to long maturities (Table 2).

To assess how return volatility varied around the rise and fall of the Nasdaq, Figure 1 plots the time series of the return volatility $\sqrt{V_t}$, represented in volatility percentage points, and contrasts it with the time series of the Nasdaq 100 tracking stock from March 1999 to April 2001. The solid line represents the volatility time series, with units displayed on the left side of the y-axis, and the dashed line represents the stock price time series, with units displayed on the right side of the y-axis.

During the two-year period, the Nasdaq 100 tracking stock rose from \$50 in March 1999 to \$115 in March 2000 and then fell to \$33 in April 2001. During this process, the volatility started at a relatively low level in March 1999, at about 33%, but steadily increased as the Nasdaq 100 index climbed, and reached 49% at the peak of the Nasdaq 100 valuation in March 2000.

Figure 1 reveals a positive comovement between the level of the Nasdaq 100 and its return volatility prior to the collapse of the Nasdaq market. Under normal market conditions, equity volatility tends to decline with rising equity values.

Figure 1 Return Volatility ($\sqrt{V_t}$) vs. Nasdaq Valuation

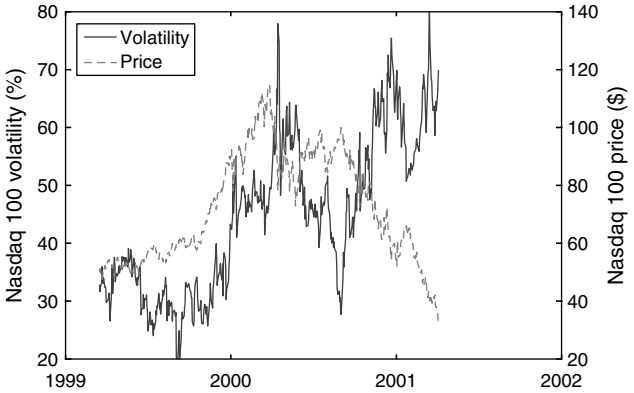

Notes. The solid line plots the daily time series of the return variance rate V_t, represented in volatility percentage points ($\sqrt{V_t}\times 100$) and with units on the left-hand side of the y-axis. The dashed line plots the time series of the daily closing price of the Nasdaq 100 tracking stock, with units on the right-hand side of the y-axis.

The volatility continued rising as the Nasdaq 100 started to fall, and peaked at 78% on April 14, 2000. The volatility remained high after the collapse of the Nasdaq in March 2000. Return volatility subsided for a few months when the Nasdaq market stabilized, but trended upward thereafter as the Nasdaq index continued its downfall. The rising Nasdaq volatility during the bubble period has also been observed by Schwert (2002) in a different context.

Several theoretical models explain how volatility can increase as a bubble builds. For example, Scheinkman and Xiong (2003) propose an equilibrium model where overconfidence generates disagreements among agents regarding asset fundamentals. These disagreements, combined with short-sale constraints, can push up both the asset price and its volatility.

5.2. Market Price of Diffusion Risk Declined with Rising Nasdaq Valuation

Panel C of Table 3 reports the coefficient estimates related to the market prices and their variations. In accordance with Equation (7) of Theorem 1, the market price of diffusion risk can be computed as $\eta_d=\gamma_B\sqrt{1-\rho^2}+\gamma_Z\rho$. The estimate for the market price of diffusion return risk γ_B is positive at 1.1209, and the estimate for the long-run mean of the diffusion variance risk $\overline{\gamma_Z}$ is -1.4325.

Given the negative correlation ρ between return and variance, both estimates contribute to an average positive diffusion return risk premium η_d of 1.82 per unit risk. This average estimate is in line with the common findings of the literature (e.g., Bliss and Panigirtzoglou 2004, Bakshi et al. 2008).

By allowing γ_Z to vary over time, the market price of diffusion return risk η_d varies accordingly. Figure 2 contrasts the variation of η_d with the Nasdaq 100 valuation during the two-year period from March 1999 to April 2001. The market price of diffusion risk started close to its average value at 1.88, and began to decline as the Nasdaq 100 price went up. From September 21, 1999, to January 5, 2000, the market price of diffusion risk reached negative territory. This period of negative market price coincided with the rising Nasdaq 100 valuation.

The market price of diffusion risk started to increase thereafter. Following the collapse of the Nasdaq market, the market price reached historically high values in May 2000, which were about twice as high as the sample average, and stayed high for a period of four months.

The market price of diffusion risk reflects either or both of (i) investors' aversion to diffusion risk and

Figure 2 Market Price of Diffusion Risk (η_d) Variation vs. Nasdaq Valuation

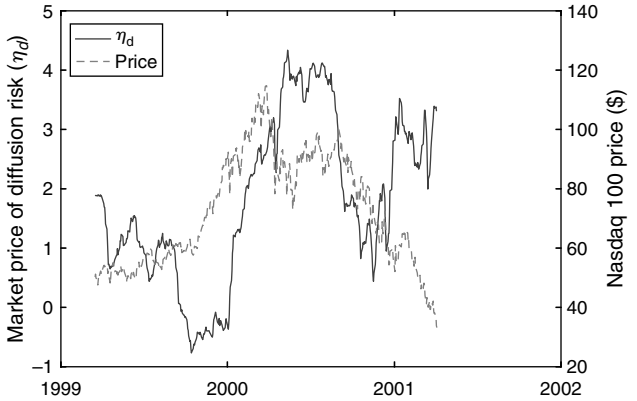

Notes. The solid line plots the daily time series of the market price of diffusion risk η_d, with units on the left-hand side of the y-axis. The dashed line plots the time series of the daily closing price of the Nasdaq 100 tracking stock, with units on the right-hand side of the y-axis. The market price of diffusion risk is computed as $\eta_d = \gamma_B\sqrt{1-\rho^2} + \gamma_Z\rho$, where (γ_B, ρ) are model parameters, and γ_Z is allowed to vary over time.

Figure 3 Market Price of Jump Risk (η_J) Variation vs. Nasdaq Valuation

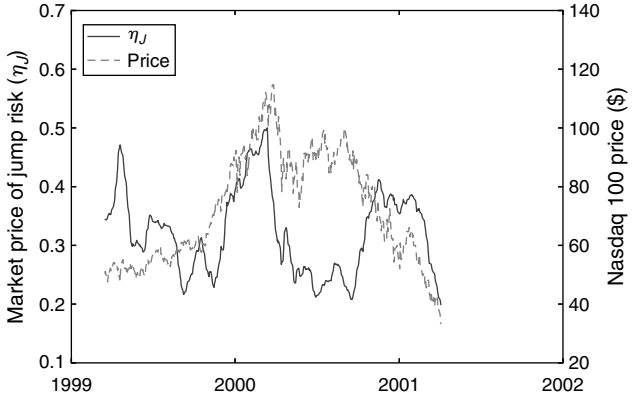

Notes. The solid line plots the daily time series of the smoothed market price of jump risk η_J, with units on the left-hand side of the y-axis. The dashed line plots the time series of the daily closing price of the Nasdaq 100 tracking stock, with units on the right-hand side of the y-axis. The market price of jump risk is computed as

$$\eta_J = \lambda(((\beta_+ - 1)^{-1} - \beta_+^{-1}) + ((\beta_- + 1)^{-1} - \beta_-^{-1})) - \lambda(((\beta_+^{\mathbb{Q}} - 1)^{-1} - (\beta_+^{\mathbb{Q}})^{-1}) + ((\beta_-^{\mathbb{Q}} + 1)^{-1} - (\beta_-^{\mathbb{Q}})^{-1})),$$

where $(\lambda, \beta_+, \beta_-)$ are constant model parameters, and $(\beta_+^{\mathbb{Q}}, \beta_+^{\mathbb{Q}})$ are allowed to vary over time.

(ii) deviations of investors' subjective beliefs from statistical realities about future cash flows. The negative market price estimates before 2000 highlight a combination of the market's appetite for risk and an exaggerated view of future cash flows that coincided with the trending Nasdaq valuation. On the other hand, the highly positive market price estimates after the Nasdaq collapse reflect investors' renewed aversion to diffusive risk and a realigned projection about future cash flow.

5.3. Market Price of Jump Risk Rose with Nasdaq 100 Valuation

Combining Equations (8) and (13), we can express the market price of jump risk as

$$\eta_J = \lambda(((\beta_+ - 1)^{-1} - \beta_+^{-1}) + ((\beta_- + 1)^{-1} - \beta_-^{-1})) - \lambda(((\beta_+^{\mathbb{Q}} - 1)^{-1} - (\beta_+^{\mathbb{Q}})^{-1}) + ((\beta_-^{\mathbb{Q}} + 1)^{-1} - (\beta_-^{\mathbb{Q}})^{-1})). \quad (35)$$

Table 3 reports the parameter estimates on the jump characteristics $(\lambda, \beta_+, \beta_-)$ in panel B and the average of the risk-neutral counterparts $(\overline{\ln\beta_+^{\mathbb{Q}}}, \overline{\ln\beta_+^{\mathbb{Q}}})$ in panel C. These estimates imply an average jump risk premium of 0.1033 per unit risk, considerably smaller than the average estimate for the diffusion risk.

Based on the extracted time series on $(\ln\beta_+^{\mathbb{Q}}, \ln\beta_-^{\mathbb{Q}})$, we compute the time series on the market price of jump risk η_J via (35). Figure 3 contrasts its variation with the rise and fall of the Nasdaq 100 valuation from March 1999 to April 2001. Given the data noise on deep OTM options, the daily estimates for the market price of jump risk appear to be noisy. To obtain a clearer pattern for the time variation, we apply an exponential smoothing on the daily estimates, $\eta_{J,t} = b\,\eta_{J,t-1} + (1-b)\eta_{J,t}$, where we set the smoothing coefficient to $b = 0.97$, corresponding to a half-life of about a month. The solid line in Figure 3 represents this smoothed version of the market price of jump risk.

The market price of jump risk rose sharply from late 1999 to early 2000 with the Nasdaq market, reaching its highest estimate of 0.50 in March 2000. Then, right before the collapse of the Nasdaq, the market price of the jump risk fell sharply and stayed at a relatively low level during an extended period from middle to late 2000.

5.4. Risk-Neutral Tail Asymmetry and Nasdaq Valuations

With the jump structure under the statistical measure $(\lambda, \beta_+, \beta_-)$ held invariant, the variations of the market price of jump risk η_J are driven by the relative variations of the risk-neutral jump dampening coefficients $(\beta_+^{\mathbb{Q}}, \beta_-^{\mathbb{Q}})$. A higher estimate for $\beta_+^{\mathbb{Q}}$ than for $\beta_-^{\mathbb{Q}}$ implies that the left tail of the risk-neutral return innovation distribution is heavier than the right tail. Therefore, we can measure the risk-neutral tail asymmetry by the difference in the dampening coefficients, $NSKEW^{\mathbb{Q}} \equiv (\beta_+^{\mathbb{Q}} - \beta_-^{\mathbb{Q}})$, which is another way to assess how expensive OTM put options are relative to OTM call options of comparable moneyness. A higher difference translates into a more negatively skewed risk-neutral return innovation distribution.

Figure 4 Variation of Risk-Neutral Tail Asymmetry vs. Nasdaq Valuation

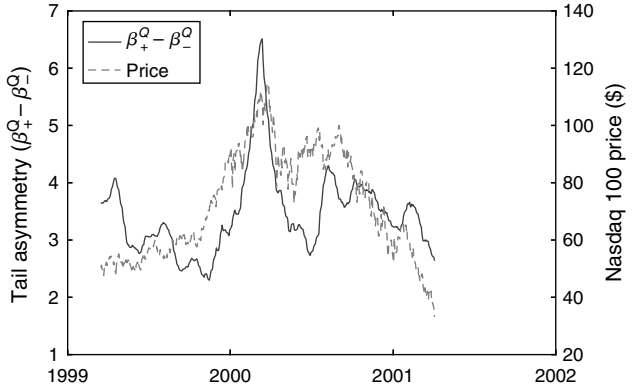

Notes. The solid line plots the daily time series of the smoothed risk-neutral tail asymmetry measure, $NSKEW^{\mathbb{Q}} = \beta_+^{\mathbb{Q}} - \beta_-^{\mathbb{Q}}$, with units on the left-hand side of the y-axis. The dashed line plots the time series of the daily closing price of the Nasdaq 100 tracking stock, with units on the right-hand side of the y-axis. $\beta_+^{\mathbb{Q}}$ and $\beta_-^{\mathbb{Q}}$ are the dampening coefficients under the risk-neutral measure of upside and downside jumps, respectively. A positive estimate for $NSKEW^{\mathbb{Q}}$ indicates a negative skewness for the risk-neutral return innovation distribution.

Figure 4 plots the time series of $NSKEW^{\mathbb{Q}}$ estimates and contrasts its variation with that of the Nasdaq 100 tracking stock. As with the market price of jump risk, we smooth the daily $NSKEW^{\mathbb{Q}}$ estimates to remove the temporal noise.

The difference $NSKEW^{\mathbb{Q}}$ has stayed positive during the whole sample period, indicating that OTM puts have been more expensive than the corresponding OTM calls, and that the left tail of the return innovation has been heavier than the right tail. What may be more informative, however, is the observation that this price asymmetry increased as rapidly as the price rise of the Nasdaq 100 tracking stock. OTM put options became increasingly expensive as the underlying stock price increased.

Because OTM put options are natural instruments for hedging against market crashes, it is possible that as the Nasdaq 100 rose, investors became increasingly worried about its sustainability and started to buy OTM put options to hedge against a potential collapse. The buying pressure raised the OTM put prices more than it did the OTM call prices, thus generating a more negatively skewed risk-neutral return distribution.

5.5. Supporting Evidence from Open Interest on Puts and Calls

To gauge whether the observed risk-neutral tail asymmetry is supported by the demand imbalance for different types of options contracts, we retrieve the daily aggregate open interest data from OptionMetrics for calls and puts on the Nasdaq 100 tracking stock. Figure 5 plots the time series of the open interest on calls ($OPEN_t^{\text{call}}$) and puts ($OPEN_t^{\text{put}}$), where the two series

Figure 5 Put and Call Open Interest Variation

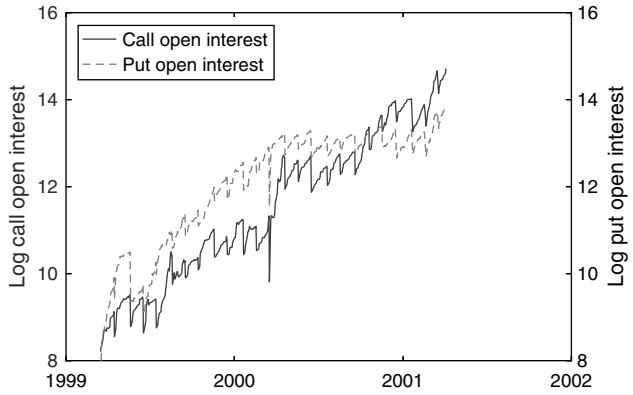

Notes. The solid line plots the daily time series of call open interest ($OPEN_t^{\text{call}}$, in logarithms), with units on the left-hand side of the y-axis. The dashed line plots the daily time series of the put open interest ($OPEN_t^{\text{put}}$, in logarithms), with units on the right-hand side of the y-axis.

are expressed in natural logs of the aggregate number of contracts.

The plot shows a steady increase of daily open interest for both calls and puts. From the start of the sample in March 1999 to mid 2000, the open interest for puts are higher than that for calls. After that, we observe a reversal in the demand, with more open interest for calls than for puts. Over the whole sample period, the average open interest for calls are higher than for puts. The same average imbalance pattern holds for the selected options sample used for model estimation (Table 2).

To highlight the time variation of the imbalance between the call and put open interests, we define a put–call open interest imbalance measure as

$$IMBAL_t \equiv \frac{OPEN_t^{\text{put}} - OPEN_t^{\text{call}}}{OPEN_t^{\text{put}} + OPEN_t^{\text{call}}}. \tag{36}$$

Figure 6 plots the time series of the open interest imbalance measure and contrasts it with the rise and fall of the Nasdaq 100 tracking stock. The imbalance started negative, but quickly turned positive and reached extreme positive levels before the collapse of the market. The imbalance became as high as 74.73% at the peak of the Nasdaq 100 valuation on March 10, 2000. On that date, call options had an open interest of 54,150 contracts, whereas put options had an open interest of 374,452 contracts, close to seven times as much as the call open interest.

The open interest imbalance declined rapidly after the peak of the Nasdaq. It reduced to about 30% a month after the peak, turning negative by October of 2000 and staying mostly negative thereafter.

The variations of the open interest imbalance are largely consistent with the variations of the risk-neutral tail asymmetry and support our conjecture on the hedging motive of investors. While there is a

Figure 6 Put–Call Open Interest Imbalance vs. Nasdaq Valuation

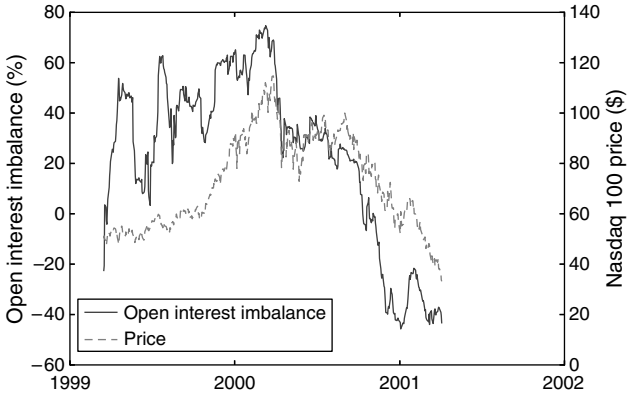

Notes. The solid line plots the daily time series of the put–call open interest imbalance, $IMBAL_t \equiv (OPEN_t^{\text{put}} - OPEN_t^{\text{call}})/(OPEN_t^{\text{put}} + OPEN_t^{\text{call}})$, with units on the left-hand side of the y-axis, where $OPEN_t^{\text{call}}$ and $OPEN_t^{\text{put}}$ denote the call and put open interest, respectively. The dashed line plots the time series of the daily closing price of the Nasdaq 100 tracking stock, with units on the right-hand side of the y-axis.

higher demand for call options than for put options on average, the demand for put options outweighed the demand for call options as the Nasdaq 100 trended upward in late 1999 and early 2000. The asymmetries in both option prices and open interests were released only after the collapse of the Nasdaq market.

6. Concluding Remarks

This paper develops a theoretical and empirical framework to study the variations of risk and market prices of different sources of risk over the Nasdaq bubble period. Our model estimation identifies three major variations in the Nasdaq 100 tracking stock during the bubble period.

First, return volatility as a risk measure increased with the rising valuation of the Nasdaq 100, even though the two tend to move in opposite directions under normal market conditions.

Second, the estimates for the market price for diffusion risk average around 1.82, close to common findings in the literature, but the estimates became negative from September 21, 1999, to January 5, 2000, as the Nasdaq index rose.

Third, the market price of jump risk became unusually high as the bubble built up. This elevated market price is a result of Nasdaq 100 puts becoming more expensive than calls during this period, which we trace to the imbalance in their respective open interests. Although call options on average have higher open interest and trading volume than put options for the Nasdaq 100 tracking stock, the open interest for put options, which can be used for hedging market crashes, became much higher than the open interest for calls as the Nasdaq 100 price became increasingly unsustainable.

The presence of options trading on the Nasdaq 100 tracking stock enhances our identification of all three pieces of evidence. By combining the information in option prices across all strikes and maturities with the time-series returns on the index tracking stock, we have achieved a sharper separation of different sources of risk and the market price on each risk source.

Although the focal point of this paper is the Nasdaq bubble, our framework can be adapted to probe the variations in the risk level and market prices of risk during other bubble periods, when options on an underlying index are available. A concrete example is the U.S. national home price index, which rose from 100 to 189 from 2000 to 2006, and then collapsed to 129 in the last quarter of 2008. One can perform an analogous analysis to gain insights about the risk and market price variations from options written on a housing index.

Acknowledgments

The authors thank Andrew Ang, Peter Carr, Fousseni Chabi-Yo, Xiaohui Gao, Soeren Hvidkjaer, Nengjiu Ju, Nikunj Kapadia, Alok Kumar, Pete Kyle, Mark Loewenstein, Dilip Madan, George Panayotov, Neil Pearson, George Pennacchi, Allen Poteshman, Hersh Shefrin, Andrei Simonov, Georgios Skoulakis, Rene Stulz, Hao Zhou, and seminar participants at the 2006 Western Finance Association meetings in Colorado, the BSI Gamma Foundation conference in Frankfurt, and the University of Illinois at Urbana-Champaign for comments. They are grateful for the feedback of Wei Xiong (the department editor), the anonymous associate editor, and two anonymous referees. Any remaining errors are their own. The 2006 version of this paper was circulated under the title "Investor Irrationality and the Nasdaq Bubble." This research was funded by BSI Gamma Foundation.

Appendix. Model Parameter Estimates Under Constant Market Prices of Risk

A. Variance risk dynamics

	κ	θ	ω	ρ
Coef.	7.3414	0.1027	0.8207	−0.7305
t-statistic	(77.96)	(82.95)	(110.12)	(−86.96)

B. Jump risk dynamics

	λ	β_+	β_-
Coef.	51.4936	11.4948	44.3947
t-statistic	(42.15)	(1.74)	(0.04)

C. Market prices of diffusion and jump risks

	γ_Z	γ_B	$\beta_+^{\mathbb{Q}}$	$\beta_-^{\mathbb{Q}}$
Coef.	−1.394	1.0813	10.4899	6.9343
t-statistic	(−12.99)	(0.52)	(145.17)	(138.9)

Appendix. (Continued)

D. Cross-sectional and serial dependence in measurement errors

	g_d	g_m	ρ_e	σ_e^2
Coef.	1.1157	0.1061	0.4352	0.054
t-statistic	(686.29)	(97.78)	(150.24)	(225.65)

Notes. Entries report the maximum likelihood estimates of the model parameters under the assumption of constant market prices of risk. The t-statistics are shown in parentheses. The estimation is based on daily time-series returns and option prices on Nasdaq 100 tracking stock over the sample period from March 17, 1999, to February 19, 2003. Likelihoods on the options are constructed by assuming normally distributed options forecasting errors, with the mean and covariance of the forecasts obtained from the unscented Kalman filter. Likelihoods on daily returns are computed by inverting the characteristic function of the daily return, conditional on the variance rate extracted from the options. The joint likelihood is obtained by assuming independence between options forecasting errors and daily stock returns.

References

Abreu, D., M. Brunnermeier. 2003. Bubbles and crashes. *Econometrica* **71**(3) 173–204.

Aït-Sahalia, Y., A. Lo. 1998. Nonparametric estimation of state-price densities implicit in financial asset prices. *J. Finance* **53**(2) 499–547.

Bakshi, G., C. Cao, Z. Chen. 1997. Empirical performance of alternative option pricing models. *J. Finance* **52**(5) 2003–2049.

Bakshi, G., P. Carr, L. Wu. 2008. Stochastic risk premiums, stochastic skewness in currency options, and stochastic discount factors in international economies. *J. Financial Econom.* **87**(1) 132–156.

Battalio, R., P. Schultz. 2006. Options and the bubble. *J. Finance* **61**(5) 2071–2102.

Birru, J., S. Figlewski. 2009. Anatomy of a meltdown: The risk neutral density for the S&P 500 in the fall of 2008. Working paper, New York University, New York.

Black, F., M. Scholes. 1973. The pricing of options and corporate liabilities. *J. Political Econom.* **81**(3) 637–654.

Bliss, R. R., N. Panigirtzoglou. 2004. Option-implied risk aversion estimates. *J. Finance* **59**(1) 407–446.

Bollen, N., R. Whaley. 2004. Does net buying pressure affect the shape of implied volatility functions? *J. Finance* **59**(2) 711–753.

Bollerslev, T. 1986. Generalized autoregressive conditional heteroskedasticity. *J. Econometrics* **31**(3) 307–327.

Bollerslev, T., V. Todorov. 2009. Tails, fears, and risk premia. Working paper, Duke University, Durham, NC.

Brunnermeier, M., S. Nagel. 2004. Hedge funds and the technology bubble. *J. Finance* **59**(5) 2013–2040.

Carr, P., D. Madan. 1999. Option valuation using the fast Fourier transform. *J. Comput. Finance* **2**(4) 61–73.

Carr, P., L. Wu. 2004. Time-changed Lévy processes and option pricing. *J. Financial Econom.* **71**(1) 113–141.

Christoffersen, P., K. Jacobs, C. Ornthanalai, Y. Wang. 2008. Option valuation with long-run and short-run volatility components. *J. Financial Econom.* **90**(3) 272–297.

Dhar, R., W. N. Goetzmann. 2005. Bubble investors: What were they thinking? Yale ICF Working Paper 05-01, Yale International Center for Finance, Yale School of Management, New Haven, CT.

Engle, R. F. 1982. Autoregressive conditional heteroskedasticity with estimates of the variance of United Kingdom inflation. *Econometrica* **50**(4) 987–1007.

Figlewski, S. 2009. Estimating the implied risk neutral density for the U.S. market portfolio. T. Bollerslev, J. R. Russell, M. Watson, eds. *Volatility and Time Series Econometrics: Essays in Honor of Robert F. Engle*. Oxford University Press, Oxford, UK, 323–353.

Garber, P. 1989. Tulipmania. *J. Political Econom.* **97**(3) 535–560.

Griffin, J., J. Harris, S. Topaloglu. 2004. Who drove and burst the tech bubble? Working paper, University of Texas, Austin.

Heston, S. 1993. Closed-form solution for options with stochastic volatility, with application to bond and currency options. *Rev. Financial Stud.* **6**(2) 327–343.

Hong, H., J. Scheinkman, W. Xiong. 2006. Asset float and speculative bubbles. *J. Finance* **61**(3) 1073–1117.

Huang, J., L. Wu. 2004. Specification analysis of option pricing models based on time-changed Lévy processes. *J. Finance* **59**(3) 1405–1440.

Jones, C. 2006. A nonlinear factor analysis of S&P 500 index option returns. *J. Finance* **61**(5) 2325–2363.

Kalman, R. E. 1960. A new approach to linear filtering and prediction problems. *Trans. ASME J. Basic Engrg.* **82**(Series D) 35–45.

Kindleberger, C. 2000. *Manias, Panics, and Crashes: A History of Financial Crises*, 4th ed. John Wiley & Sons, New York.

Kou, S. 2002. A jump-diffusion model for option pricing. *Management Sci.* **48**(8) 1086–1101.

Küchler, U., M. Sørensen. 1997. *Exponential Families of Stochastic Processes*. Springer, New York.

Lakonishok, J., I. Lee, N. Pearson, A. Poteshman. 2007. Option market activity. *Rev. Financial Stud.* **20**(3) 813–857.

Lamont, O., R. Thaler. 2003. Can the market add and subtract? Mispricing in tech stock carve-outs. *J. Political Econom.* **58**(3) 1113–1138.

LeRoy, S. 2004. Rational exuberance. *J. Econom. Literature* **42**(3) 783–804.

Li, H., M. Wells, L. Yu. 2008. A Bayesian analysis of return dynamics with Lévy jumps. *Rev. Financial Stud.* **21**(5) 2345–2378.

Merton, R. C. 1976. Option pricing when underlying stock returns are discontinuous. *J. Financial Econom.* **3**(1) 125–144.

Ofek, E., M. Richardson. 2002. The valuation and market rationality of Internet stock prices. *Oxford Rev. Econom. Policy* **18**(3) 265–287.

Ofek, E., M. Richardson. 2003. DotCom mania: The rise and fall of Internet stock prices. *J. Finance* **58**(3) 1113–1137.

Pástor, Ľ., P. Veronesi. 2006. Was there a Nasdaq bubble in the late 1990s? *J. Financial Econom.* **81**(1) 61–100.

Santa-Clara, P., S. Yan. 2010. Crashes, volatility, and the equity premium: Lessons from S&P 500 index options. *Rev. Econom. Statist.* **92**(2) 435–451.

Scheinkman, J., W. Xiong. 2003. Overconfidence and speculative bubbles. *J. Political Econom.* **111**(6) 1183–1219.

Schwert, G. W. 2002. Stock volatility in the new millennium: How wacky is Nasdaq? *J. Monetary Econom.* **49**(1) 3–26.

Temin, P., H.-J. Voth. 2004. Riding the South Sea bubble. *Amer. Econom. Rev.* **94**(5) 1654–1668.

Wan, E. A., R. van der Merwe. 2001. The unscented Kalman filter. S. Haykin, ed. *Kalman Filtering and Neural Networks*, Chap. 7. John Wiley & Sons, New York, 221–280.